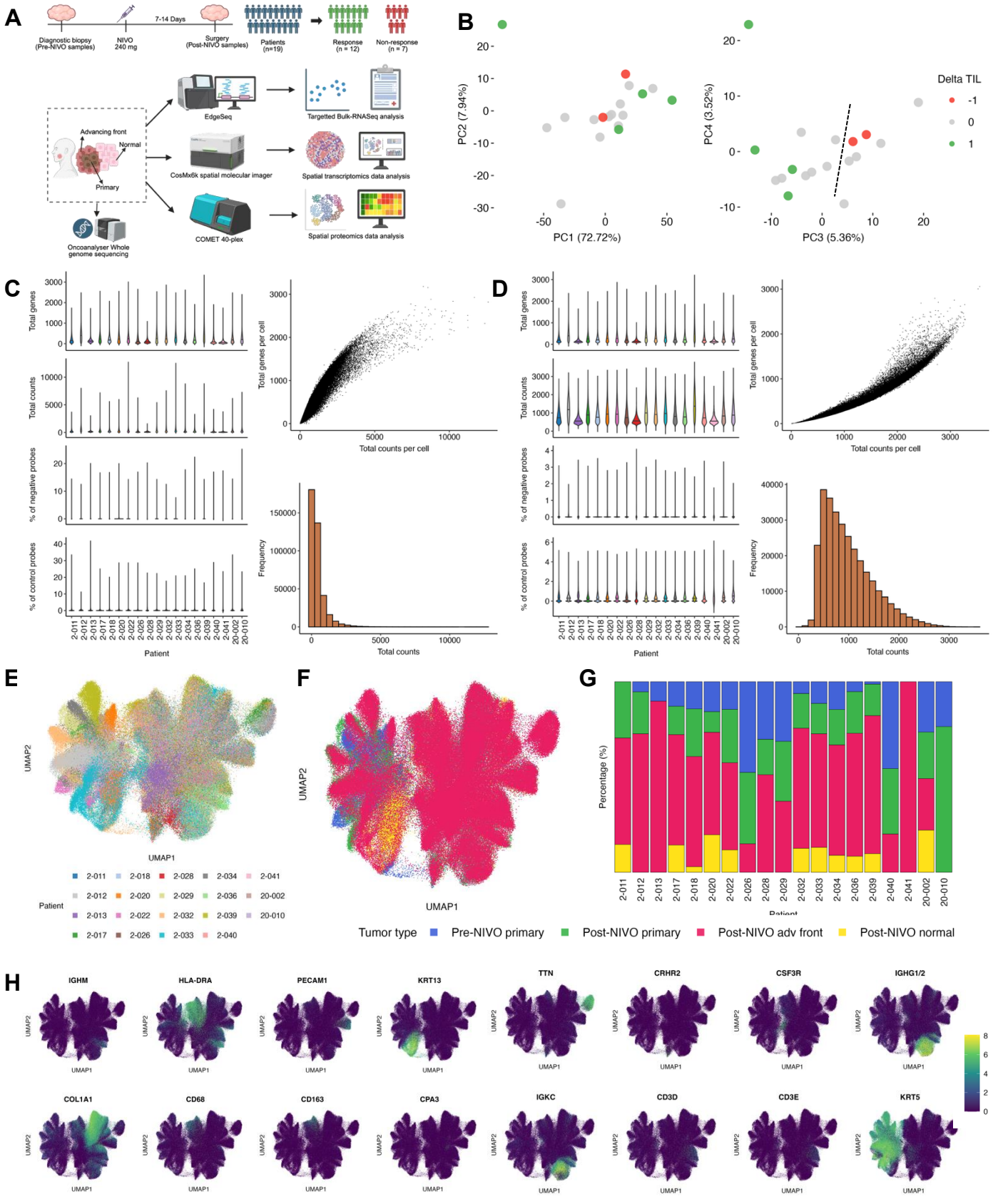

Supp Figure 2. Cohort overview, quality control, and integration of CosMx6k spatial transcriptomic data.
(A) Study schematic illustrating cohort design, treatment timeline, tumour sampling strategy, and multi-omics profiling workflow.
(B) Principal component analysis (PCA) of patient-specific bulk RNA-seq log2 fold-change profiles across the first four principal components (PC1–PC4). Each point represents one patient and is coloured by ΔTIL. The dashed line in the PC3 panel indicates the decision boundary used to classify patients into the Response and Non-response groups.
(C) Summary of quality-control metrics for the raw CosMx spatial transcriptomic dataset, comprising patient-level QC metrics (total genes, total transcript counts, negative probe percentages and control probe percentages), a scatter plot of total genes per cell versus total transcript counts per cell, and a histogram of total transcript counts.
(D) Summary of quality-control metrics for the pre-processed CosMx spatial transcriptomic dataset, comprising patient-level QC metrics (total genes, total transcript counts, negative probe percentages and control probe percentages), a scatter plot of total genes per cell versus total transcript counts per cell, and a histogram of total transcript counts.
(E) UMAP representation of the CosMx 6K single-cell spatial transcriptomic dataset, coloured by patient identity
(F) UMAP representation of the CosMx 6K single-cell spatial transcriptomic dataset, coloured by Tumor type
(G) Stacked bar plot showing the relative cell type composition across Tumor type
(H) UMAP representation of canonical marker gene expression across the CosMx 6K single-cell spatial transcriptomic dataset.

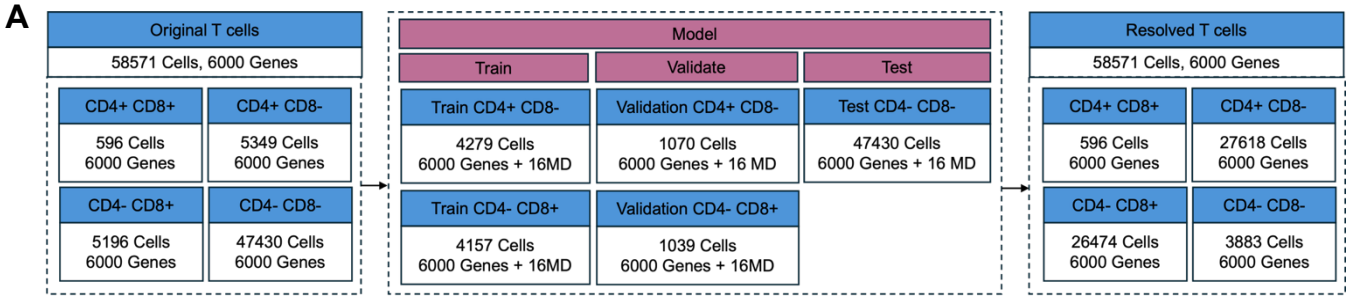

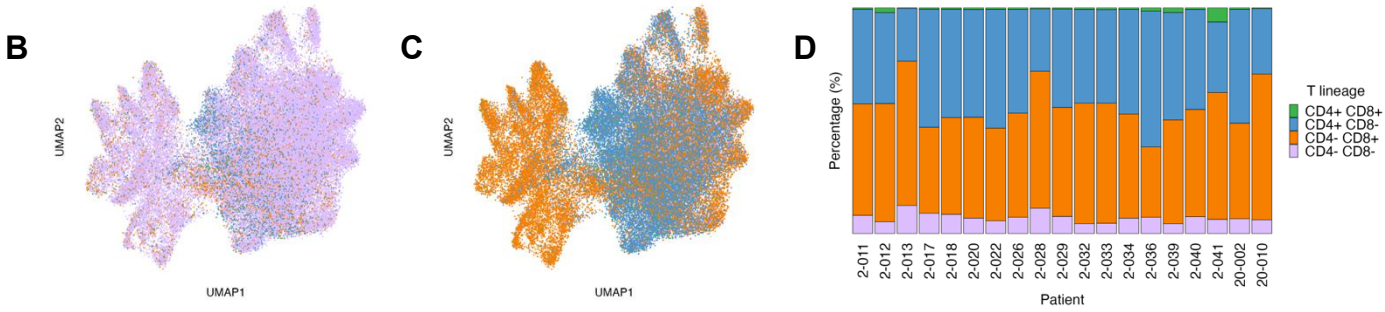

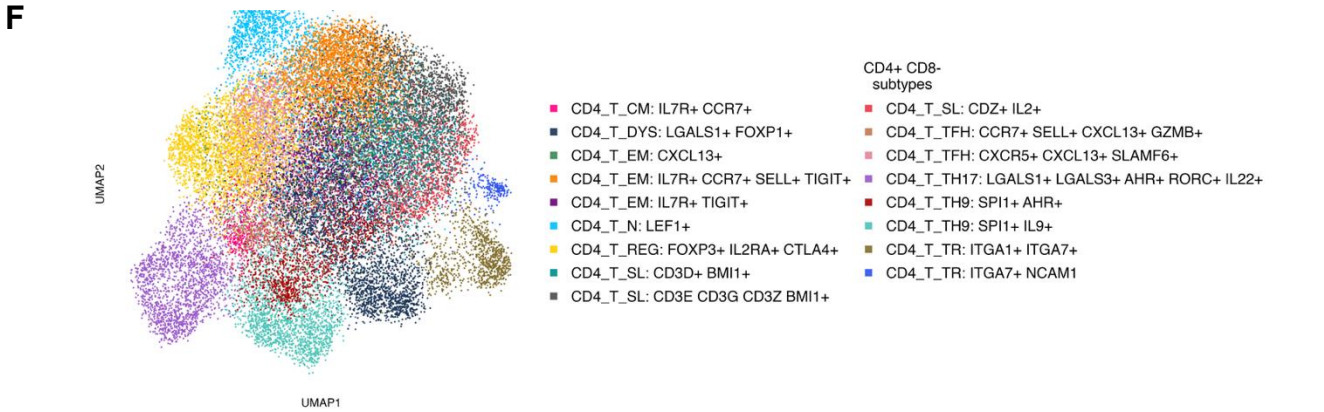

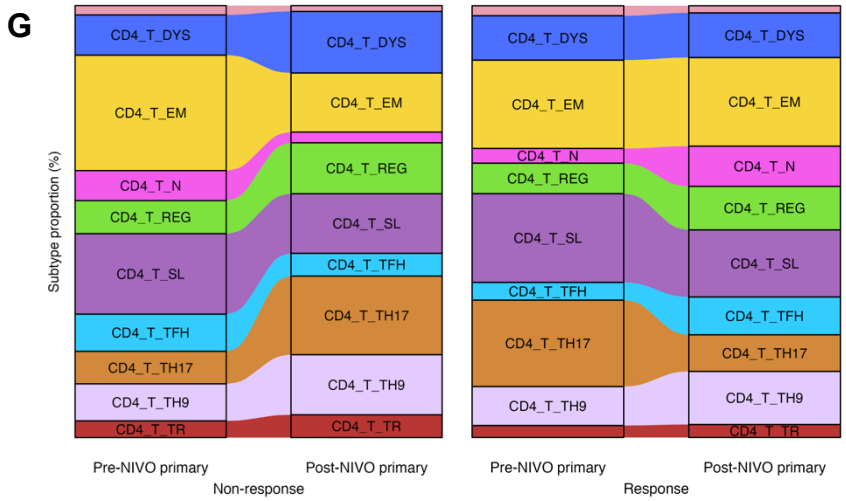

Supp Figure 3. Computational T cell lineage resolution and supplementary characterization of CD8⁺ and CD4⁺ T cell subtypes.
(A) Workflow for random forest–based classification of CD4⁻CD8⁻ T cells into CD4⁺CD8⁻ and CD4⁻CD8⁺ T cell lineages.
(B) UMAP representation of T cells before lineage resolution.
(C) UMAP representation of T cells following lineage resolution, showing improved separation of CD4⁺CD8⁻ and CD4⁻CD8⁺ T cell populations.
(D) Stacked bar plot showing the percentage of each resolved T cell lineage in individual patients.
(E) UMAP representation of CD8⁺ T cells coloured by finer-grained subtype annotation, highlighting transcriptionally distinct subpopulations within the major CD8⁺ T cell subtypes.
(F) UMAP representation of CD4⁺ T cells coloured by finer-grained subtype annotation, highlighting transcriptionally distinct subpopulations within the major CD4⁺ T cell subtypes.
(G) Alluvial plots illustrating treatment-associated changes in CD4⁺ T cell subtype proportions between pre-NIVO and post-NIVO primary tumour samples, pooled across patients within the Response and Non-response groups.

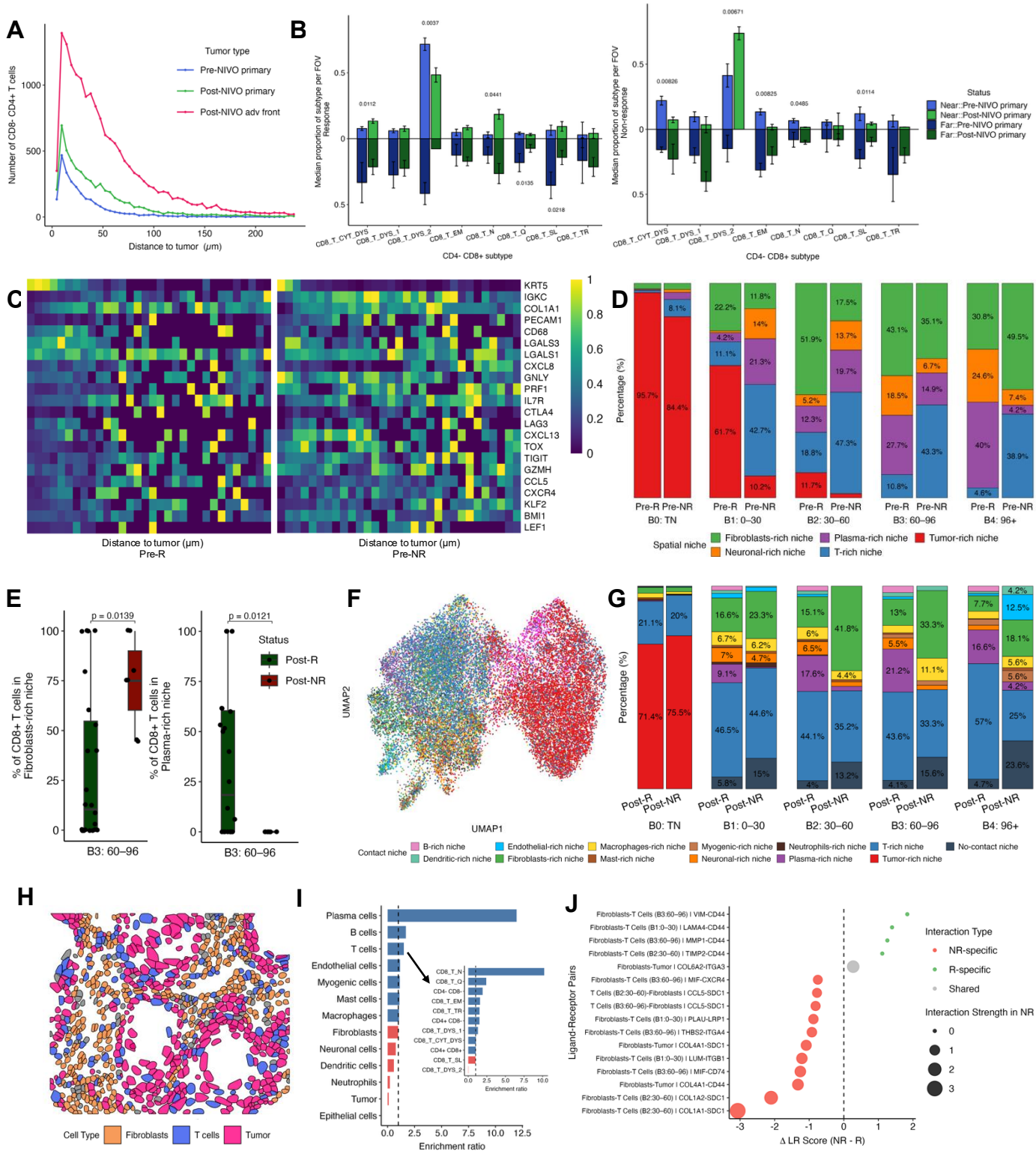

Supp Figure 4. Supplementary analyses supporting spatial organization, niche composition and ligand–receptor interactions of CD8⁺ T cells.
(A) Line plot showing the distribution of CD4⁺ T cells as a function of distance to tumour (μm) across pre-NIVO primary, post-NIVO primary and post-NIVO advancing front tumour samples.
(B) Mirrored bar plots showing the proportions of CD8⁺ T cell subtypes in near- and far-tumour regions across pre-NIVO and post-NIVO primary tumour samples. Bars represent the median proportion across fields of view (FOVs), error bars indicate standard deviations, and statistical comparisons were performed using Wilcoxon rank-sum tests.
(C) Heatmaps showing spatial gene expression gradients across distance-to-tumour bins in pre-NIVO primary tumour samples from the Response (Pre-R) and Non-response groups (Pre-NR). Gene expression was min–max normalized across distance bins for each gene.
(D) Stacked bar plots showing the proportions of CD8⁺ T cell spatial niches across distance-to-tumour bins in pre-NIVO Response and pre-NIVO Non-response primary tumour samples.
(E) Box plots showing the percentage of CD8⁺ T cells localized within fibroblast-rich and plasma cell-rich niches in the B3 (500–800 μm) distance-to-tumour compartment of post-NIVO primary tumour samples. Each dot represents one tissue core. Statistical comparisons were performed using Wilcoxon rank-sum tests.
(F) UMAP representation of CD8⁺ T cells coloured by contact-based niche annotation.
(G) Stacked bar plots showing the proportions of contact-based CD8⁺ T cell niches across distance-to-tumour bins in post-NIVO Response and post-NIVO Non-response primary tumour samples.
(H) Representative spatial reconstruction from a Non-response sample showing CD8⁺ T cells embedded within a fibroblast-rich niche.
(I) Enrichment ratio analysis of neighbouring cell populations surrounding CD8⁺ T cells in direct contact with plasma cells relative to all other CD8⁺ T cells. The left panel summarizes enrichment across major cell types, while the right panel shows the corresponding enrichment of CD8⁺ T cell subtypes.
(J) Differential spatial ligand–receptor interaction analysis (ΔLR = NR − R) between tumour cells, fibroblasts and CD8⁺ T cells across distance-to-tumour bins. Positive values indicate interactions enriched in the Response group, whereas negative values indicate interactions enriched in the Non-response group.

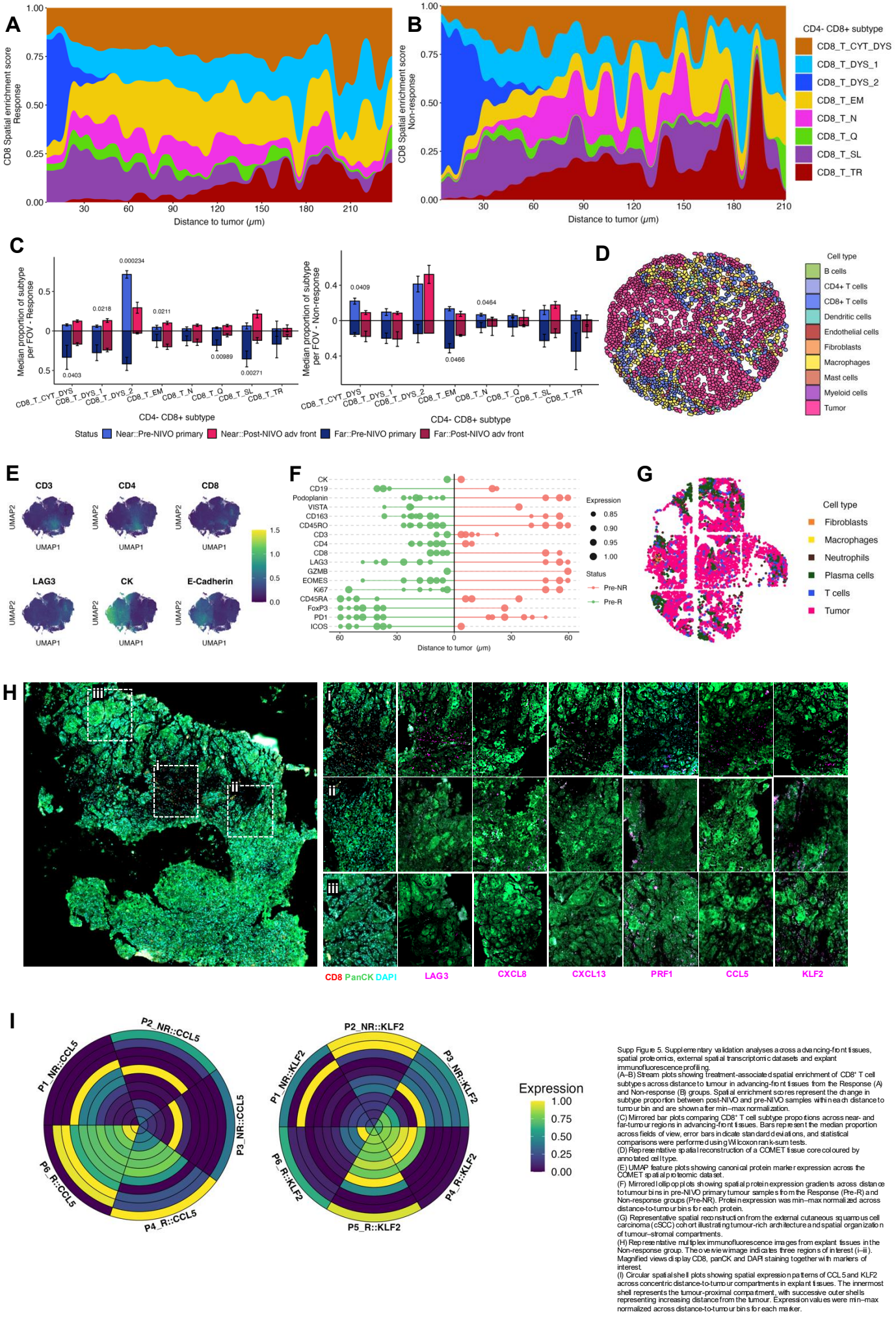

Supp Figure 5. Supplementary validation analyses across advancing-front tissues, spatial proteomics, external spatial transcriptomic datasets and explant immunofluorescence profiling.
(A–B) Stream plots showing treatment-associated spatial enrichment of CD8⁺ T cell subtypes across distance to tumour in advancing-front tissues from the Response (A) and Non-response (B) groups. Spatial enrichment scores represent the change in subtype proportion between post-NIVO and pre-NIVO samples within each distance to tumour bin and are shown after min–max normalization.
(C) Mirrored bar plots comparing CD8⁺ T cell subtype proportions across near- and far-tumour regions in advancing-front tissues. Bars represent the median proportion across fields of view, error bars indicate standard deviations, and statistical comparisons were performed using Wilcoxon rank-sum tests.
(D) Representative spatial reconstruction of a COMET tissue core coloured by annotated cell type.
(E) UMAP feature plots showing canonical protein marker expression across the COMET spatial proteomic dataset.
(F) Mirrored lollipop plots showing spatial protein expression gradients across distance to tumour bins in pre-NIVO primary tumour samples from the Response (Pre-R) and Non-response groups (Pre-NR). Protein expression was min–max normalized across distance-to-tumour bins for each protein.
(G) Representative spatial reconstruction from the external cutaneous squamous cell carcinoma (cSCC) cohort illustrating tumour-rich architecture and spatial organization of tumour–stromal compartments.
(H) Representative multiplex immunofluorescence images from explant tissues in the Non-response group. The overview image indicates three regions of interest (i–iii). Magnified views display CD8, panCK and DAPI staining together with markers of interest.
(I) Circular spatial shell plots showing spatial expression patterns of CCL5 and KLF2 across concentric distance-to-tumour compartments in explant tissues. The innermost shell represents the tumour-proximal compartment, with successive outer shells representing increasing distance from the tumour. Expression values were min–max normalized across distance-to-tumour bins for each marker.